

Testing kinetically coupled inflation models with CMB distortions

Rui Dai¹ and Yi Zhu^{1,*}

¹*School of Science, Wuhan University of Technology, Wuhan 430070, China*

(Dated: November 15, 2019)

Inflation scenarios kinetically coupled with the Einstein tensor have been widely studied. They can be consistent with current observational data. Future experiments on the measurement on CMB distortions will potentially extend information about the scalar spectrum to small scales $1\text{Mpc}^{-1} \lesssim k \lesssim 2 \times 10^4\text{Mpc}^{-1}$. By taking the sensitivity of the PIXIE experiment as criterion, we perform a model-oriented analysis of the observational prospects of spectral distortions for kinetically coupled inflation. There are five models that can generate a detectable level of distortions, among the 49 single-field inflation models listed in Ref. [1]. These models are: hybrid inflation in the valley (VHI), non-canonical Kähler inflation (NCKI), generalized MSSM inflation (GMSSMI), generalized renormalization point inflation (GRIPI), and running-mass inflation (RMI). Each of these models can induce 5σ detectable signals in a tuned region of their parameter space. The existence of kinetic coupling suppresses the value of the model parameters with mass dimension for VHI, GMSSMI, and GRIPI, such that these three models can be in agreement with their theoretical considerations.

PACS numbers: 98.80.Cq

I. INTRODUCTION

In the last three decades, observations of the anisotropies of the Cosmic Microwave Background (CMB) and the inhomogeneities of Large Scale Structure (LSS) have provided strong evidence for cosmic inflation. At the same time, they also bring stringent constraints to the sharpness and amplitude of the power spectrum of primordial fluctuations at scales where $k \geq 3\text{Mpc}$. Combining the latest observational data from the PLANCK satellite [2, 3], the scalar amplitude is required to be $P_\zeta \simeq 2.10 \times 10^{-9}$, the spectral index $n_s \simeq 0.965$, and the tensor to scalar ratio $r_{0.002} < 0.10$. Many inflation models have been ruled out or strongly disfavored, such as minimally coupled Higgs inflation, power law inflation with ϕ^4 , and original hybrid model. However, a large number of models still survive. Our knowledge about the details of inflation is limited, especially for its behavior at small scales. There are only upper limits for the primordial curvature perturbations from observations of ultra-compact minihalos [4] and primordial black holes [5].

In order to extend the available information on the inflation at small scales, some other signals and observational measurements, such as the 21 cm radiation from the dark age [6–8], and spectral distortions of the CMB [9, 10], are being seriously considered. Generally speaking, spectral distortions can be produced by energy exchange between CMB photons and matter with several physical mechanisms [11–14], e.g., the decay or annihilation of relic particles, the evaporation of primordial black holes, dissipation of primordial acoustic modes, the thermal Sunyaev-Zeldovich effect after recombination, and dark matter annihilation. Among these processes, distortions caused by the damping of primordial perturbations are relevant to the inflationary epoch. In addition, there is an observational frequency window at about 200GHz for this damping signal, c.f. Ref. [15]. Observations on distortion can provide information on the sharpness and amplitude of the scalar power spectrum at small scales ($1\text{Mpc}^{-1} \lesssim k \lesssim 2 \times 10^4\text{Mpc}^{-1}$). The first measurements on CMB distortions were done by the COBE/FIRAS experiment [16]. It not only gave limits on μ -type and y -type distortions as $\mu < 9 \times 10^{-5}$ and $y < 1.5 \times 10^{-5}$, but also yielded a limit on the value of the spectral index, $n_s < 1.6$ [17]. In 2011, the Primordial Inflation Explorer (PIXIE) experiment [18, 19] was proposed as part of NASA's MIDEX program. It is designed to improve the limit on CMB distortions by about three orders of magnitude. A more ambitious proposal is the Polarized Radiation Imaging and Spectroscopy Mission (PRISM) [19–21] with a sensitivity which is about ten times better than that of PIXIE. Although these two missions are not settled yet, one can still discuss the probabilities in the future experiments. In Ref. [22], the authors have performed a model-oriented analysis of the observational prospects for inflation, and find that few models can lead to detectable signals for the PIXIE experiment.

On the theoretical side, as the most general second-order scalar-tensor theory in four dimensions, Horndeski theory, have recently been investigated with many cosmological consequences [23–28]. In Horndeski theory [23, 29], the curvature tensors couple with a scalar field in 6 types in the case of four derivatives. In Ref. [30], the authors show

*Electronic address: yi.zhu@whut.edu.cn

that leaving only $Rg^{\mu\nu}\partial_\mu\phi\partial_\nu\phi$ and $R^{\mu\nu}\partial_\mu\phi\partial_\nu\phi$ terms is enough to preserve generality, and all other coupling terms are not necessary. Generally, with non-minimal derivative coupling, the order of field equation is higher than two. However, there is a ghost-free combination of these coupling terms, where the Einstein tensor $G^{\mu\nu} = R^{\mu\nu} - \frac{1}{2}g^{\mu\nu}R$ coupled with the kinetic term of the scalar field (referred as kinetic coupling). A cosmological model with this coupling term can explain both a quasi-de Sitter phase in the early universe and an exit without any fine-tuned potential [31]. For a scalar field theory without kinetic energy, the non-minimal coupled term $G^{\mu\nu}\partial_\mu\phi\partial_\nu\phi$ can behave like dark matter, whereas the scalar potential can play a role as dark energy [32]. For inflation scenarios, the non-minimal derivative coupling provides an extra friction to the rolling processes of the inflation. In this circumstance, the slow-roll conditions are easier to satisfy and the inflation process can last longer than that of the minimal coupled case. Many inflation models including those that were seemingly ruled out by observations have been re-investigated [33–37]. Curvaton scenarios and reheating processes have been reconsidered as well [38–40]. With kinetic coupling, these models can easily satisfy the constraints from CMB anisotropy observations. Therefore, it is worthwhile to investigate the non-minimally coupled inflation scenarios on the small-scale behavior of the scalar power spectrum, and weigh the possibility of inducing observational signals for future experiments.

The paper is organized as follows. In Sec. II, we briefly review the dynamics of non-minimal derivative-coupled inflation and the induced scalar power spectrum of perturbations. Sec. III is dedicated to develop criteria for observable spectral distortion signals with the sensitivity of a PIXIE-like experiment. In Secs. IV to VIII, we study the properties of CMB distortions for single field models in the high friction limit. Finally, we summarize our results and discuss the implications for future CMB distortion experiments.

II. NON-MINIMAL DERIVATIVE-COUPLED INFLATION

We consider a scalar field theory, which is kinetically coupled with the Einstein tensor. The action is given by

$$S = \frac{1}{2} \int d^4x \sqrt{-g} \left[M_{\text{pl}}^2 R - g^{\mu\nu} \partial_\mu \phi \partial_\nu \phi + \frac{1}{M^2} G^{\mu\nu} \partial_\mu \phi \partial_\nu \phi - 2V(\phi) \right] \quad (1)$$

where ϕ is the scalar field, $V(\phi)$ is its potential, M_{pl} is the reduced Planck mass, and M is the coupling constant with dimension of mass. For a spatially flat maximally symmetric spacetime, where $ds^2 = -dt^2 + a^2(t)d\Omega$, one obtains the Friedmann equation as

$$H^2 = \left(\frac{\dot{a}}{a} \right)^2 = \frac{1}{3M_{\text{pl}}^2} \left[\frac{\dot{\phi}^2}{2} \left(1 + 9\frac{H^2}{M^2} \right) + V(\phi) \right], \quad (2)$$

and the Klein-Gordon equation (equation of motion for the scalar field) as

$$\frac{d}{dt} \left[a^3 \dot{\phi} \left(1 + 9\frac{H^2}{M^2} \right) \right] = -a^3 \frac{dV}{d\phi}. \quad (3)$$

where $H \equiv \left(\frac{\dot{a}}{a} \right)$ is the Hubble expansion rate, and a dot denotes a derivative with respect to the cosmic time t .

The non-minimal derivative coupling plays a roll as a friction force, which slows down the rolling speed of the scalar field. In order to look clearly into the effect of the derivative coupling, we consider the high friction limit where $M^2 \ll H^2$. Inflation can be approximately described by a slow-roll process. The first and second slow parameters are defined respectively by

$$\epsilon = \frac{M_{\text{pl}}^2}{2} \left(\frac{V_\phi}{V} \right)^2 \frac{M^2}{3H^2}, \quad \eta = M_{\text{pl}}^2 \frac{V_{\phi\phi}}{V} \frac{M^2}{3H^2} \quad (4)$$

with $V_\phi \equiv dV/d\phi$ and $V_{\phi\phi} \equiv d^2V/d\phi^2$. The slow roll parameters are suppressed by a factor of $M^2/3H^2$. It is therefore much easier to trigger the accelerated expansion of the spacetime. In the slow roll approximation, the number of e-folds can be calculated by

$$N(\phi_*) = \int_{\phi_*}^{\phi_e} \frac{H}{\dot{\phi}} d\phi = \int_{\phi_*}^{\phi_e} \frac{1}{\sqrt{2\epsilon}} \sqrt{\frac{3H^2}{M^2}} \frac{d\phi}{M_{\text{pl}}}, \quad (5)$$

where ϕ_* and ϕ_e are the field values at horizon exit and at the end of inflation, respectively. To first order in the slow-roll parameters, the scalar power spectrum is given by

$$\mathcal{P}_\zeta(k) = \frac{H_k^2}{8\pi^2 M_{\text{pl}}^2 \epsilon_k} \left[1 + \left(\frac{1}{3} - 8C \right) \epsilon - \left(\frac{2}{3} - 2C \right) \eta \right], \quad (6)$$

and the spectral index reads

$$n_s(k) = 1 - 8\epsilon_k + 2\eta_k, \quad (7)$$

where $C \equiv \gamma_E + \ln 2 - 2 \simeq -0.7296$ and γ_E is the Euler constant. The quantities with subscript k are evaluated at the time t_k of horizon exit of the corresponding mode, i.e. when $k = a(t_k)H(t_k)$. The latest CMB anisotropies measurements give stringent constraints on the amplitude and spectral index of power spectrum. We apply the constraints from PLANCK 2018 [2, 3]. They give

$$\mathcal{P}_\zeta(k_p) = 2.10 \pm 0.03 \times 10^{-9}, \quad n_s(k_p) = 0.965 \pm 0.004, \quad (8)$$

at pivot scale $k_p = 0.05\text{Mpc}^{-1}$, which exits the horizon about 60 e-folds before the end of inflation. Since the discrepancies for the spectral index and amplitude between recent PLANCK 2018 data [2, 3] and earlier PLANCK 2013 data [41] are very small, we can make a direct comparison with the results from the minimally coupled models in Ref. [22].

III. CRITERIA FOR OBSERVABLE CMB DISTORTIONS

When scalar fluctuations re-enter into the horizon, an inevitable y -type distortion of the CMB spectrum is caused by dissipating acoustic waves in the Silk-damping tail. In the early universe, it is converted to a μ -distortion or an intermediate distortion by the thermalization process and Compton scattering. The first measurement of μ -type spectral distortion has been done by COBE/FIRAS. It gives an upper limit for the spectral index $n_s \leq 1.6$ [17]. As for future experiments, the designed sensitivity of PIXIE allows a detection of spectral distortions characterized by [18]

$$\mu = 5 \times 10^{-8} \quad \text{and} \quad y = 1 \times 10^{-8} \quad \text{at} \quad 5\sigma, \quad (9)$$

which is a thousand times improved from COBE/FIRAS. However, the damping signal is close to the detection limit of the PIXIE experiment. Using a Bayesian Markov-Chain-Monte-Carlo study with fiducial values $\mathcal{P}_\zeta^{fid}(k_d = 42\text{Mpc}^{-1} = 1.68 \times 10^{-9})$, $n_s = 0.96$ and $n_{run} = 0$, Ref. [22] suggests one take

$$\mathcal{P}_\zeta^{fid}(k_d = 42\text{Mpc}^{-1}) = 2.8 \times 10^{-9}, \quad (10)$$

as the lower limit of a 2σ detection. Therefore, observable CMB distortions must come from inflation models which satisfy PLANCK constraints at CMB anisotropy scales and give rise to an enhanced power at small scales. In addition, we do not need to consider y -distortions from the dispersion of acoustic modes, since it cannot be distinguished from the dominant contribution of the thermal Sunyaev-Zeldovich effect.

For further investigation on inflation models, we use the criteria from Ref. [22] on the scalar spectrum for potential interesting inflation models, with minor modifications:

1. There exists a locally blue tilted spectrum where $n_s > 1$. It requires that the slow-roll parameters satisfy $\eta > 4\epsilon > 0$ at some scale.
2. The scale of the blue spectrum must be smaller than that of the CMB anisotropy observations, i.e. a phase with $n_s > 1$ must follow the phase with $n_s < 1$. In order to ensure the number of e-folds never diverges, we also require that the first slow-roll parameter does not vanish.
3. We also demand inflation models generate a power spectrum with $n_s = 0.965 \pm 0.004$ at the PLANCK observation pivot scale $k_p = 0.05\text{Mpc}^{-1}$, and $n_s > 1$ at the pivot scale of CMB distortions $k_d = 42\text{Mpc}^{-1}$.

We add kinetic coupling (1) to all 49 signal field inflation models listed in Ref. [1]. By applying criteria 1 and 2, large classes of models are eliminated. Only five models survive. They are hybrid inflation in a valley, generalized MSSM inflation, generalized renormalizable inflection point inflation, non-canonical Kähler inflation, and running-mass inflation. This result is the same as that of the minimally coupled cases in Ref. [22]. The reason is that the derivative coupling gives a suppression factor $\frac{M^2}{3H^2}$ to slow roll parameters, but do not change their sign. The sign of the spectral index $n_s - 1$ is therefore preserved. For applying the third criterion, we need to numerically integrate the slow-roll dynamics for each model. In the following sections, we evaluate the scalar power spectrum for these models, and calculate the level of intermediate and μ -distortions using a modified version of the Idistort code [42].

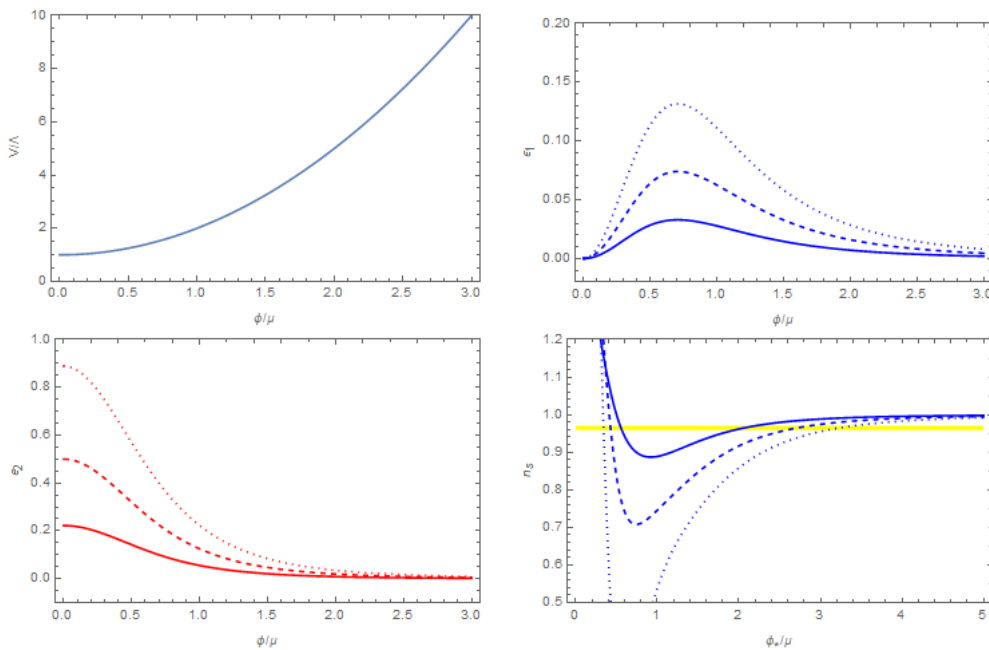


FIG. 1: Top left: original hybrid potential. Top right and bottom left: first and second slow-roll parameters ϵ and η . Bottom right: scalar spectral index n_s as a function of ϕ_k . The horizontal band corresponds to the PLANCK 95% C.L. constraints. The parameter values in the diagrams for $\epsilon_{1,2}$ and n_s are $\mu_{\text{VHI}} = 0.015M_{\text{pl}}$ (dotted), $\mu_{\text{VHI}} = 0.02M_{\text{pl}}$ (dashed) and $\mu_{\text{VHI}} = 0.03M_{\text{pl}}$ (solid). We are interested in the region close to $\phi_k/\mu_{\text{VHI}} = 1$, where the power spectrum of curvature perturbations is red-tilted, but which becomes blue-tilted a few e-folds later (i.e. at smaller values of ϕ_k .)

IV. HYBRID INFLATION IN THE VALLEY (VHI)

In the original hybrid inflation model [43], there are two scalar fields. One is the inflaton, the other is the waterfall field. Inflation takes place when the inflation rolls slowly down a potential valley. As the inflation reaches the critical point, it triggers a tachyonic waterfall phase, where the waterfall field rolls rapidly, then inflation ends. The dynamics of the inflation process can be described by an effective single field potential

$$V(\phi) = \Lambda \left(1 + \frac{\phi^2}{\mu_{\text{VHI}}^2} \right). \quad (11)$$

The potential is plotted in the top left panel of Fig. 1. The inflaton rolls from the right side towards the decreasing field values. The value of the inflaton field at the end of inflation ϕ_{end} is considered a free parameter. With the non-minimal derivative coupling $M = 0.01\sqrt{\Lambda}/M_{\text{pl}}$, the first and second slow-roll parameters are given by

$$\epsilon = \frac{M^2}{3H^2} \frac{2x^2 M_{\text{pl}}^2}{\mu^2(1+x^2)^2} = \frac{2 \times 10^{-4} x^2 M_{\text{pl}}^2}{\mu^2(1+x^2)^3}, \quad (12)$$

$$\eta = \frac{M^2}{3H^2} \frac{2M_{\text{pl}}^2}{\mu^2(x^2+1)} = \frac{2 \times 10^{-4} M_{\text{pl}}^2}{\mu^2(x^2+1)^2}, \quad (13)$$

where $x = \phi/\mu_{\text{VHI}}$. In these equations, the slow-roll approximation $3M_{\text{pl}}^2 H^2 = V$ has been applied. Slow roll parameters are also presented in Fig. 1. The first criterion from Sec. III, $\eta > 4\epsilon > 0$ can be satisfied when the field value x is small enough. In this situation, the Hubble parameter H^2 is of the same order as Λ/M_{pl}^2 , such that $M^2 \ll H^2$. It is in the high friction limit where the effects of the kinetic coupling are magnified. In addition, the spectral index as a function of ϕ_* is also plotted. From Fig. 1, one notes that the phase of the red spectrum is earlier than the phase of the blue spectrum during the inflation epoch. The non-minimal derivative-coupled hybrid inflation may therefore satisfy simultaneously PLANCK's constraints and generate an observable CMB distortion signal.

To check the third criterion, we integrate the Klein-Gordon equation numerically in slow-roll inflation, and draw a contour plot for the spectral index value in the parameter space of μ_{VHI} and ϕ_{end} in Fig. 2. The red solid lines represent the PLANCK constraints in 95% confidence level. The overlap of the region between the red lines and those

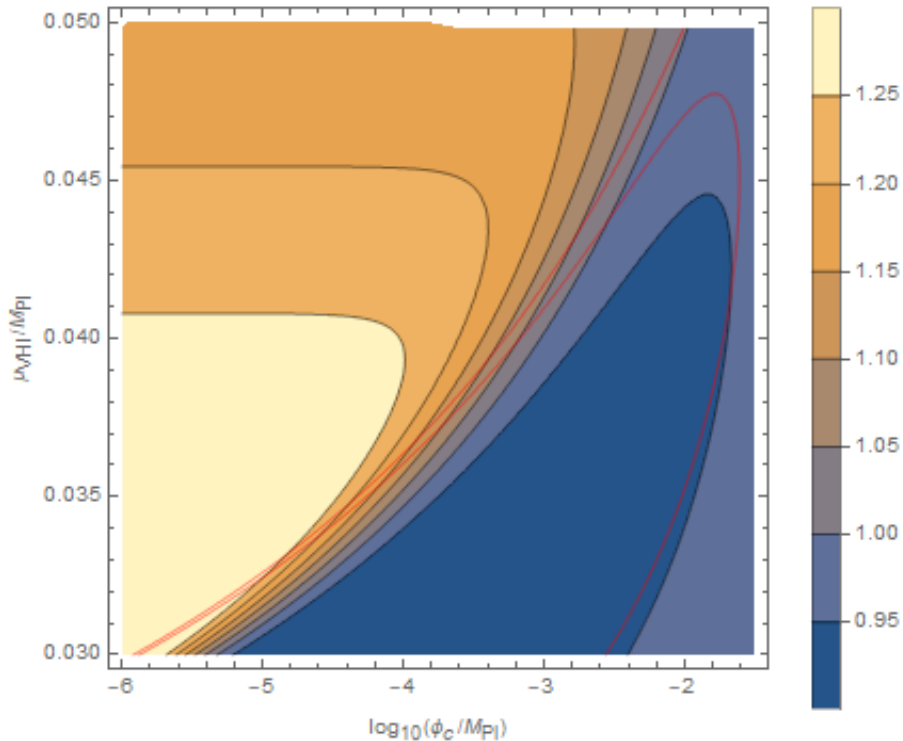


FIG. 2: Contours of spectral index values for VHI at the pivot scale of CMB distortions $k_d = 42\text{Mpc}^{-1}$. The area between the solid red lines is consistent with PLANCK constraints at 95% C.L..

of $n_s > 1$ is the region of interest. Then we choose three representative parameter sets. They are $(\mu_{VHI} = 0.0301, \log_{10} x_{end} = -5.837)$ with $n_s > 1.25$, $(\mu_{VHI} = 0.0365, \log_{10} x_{end} = -3.95)$ with $1.1 < n_s < 1.15$, and $(\mu_{VHI} = 0.0415, \log_{10} x_{end} = -3.00)$ with $n_s \simeq 1.05$. The resulting scalar power spectra as a function of the number of e-folds, and the luminosity of the CMB distortion signal as a function of frequency are plotted in Fig. 3 and Fig. 4, respectively. From the figures, we find that the larger the spectral index value is, the stronger the corresponding generated CMB distortion signal. The first parameter set leads to the strongest signal $\mu = 5.1 \times 10^{-8}$, which can be detected at more than 5σ confidence by PIXIE. In addition, we note that the level of intermediate i -distortions is much higher than that of the μ -distortions.

V. NON-CANONICAL KÄHLER INFLATION (NCKI)

Non-canonical Kähler inflation is derived from the usual hybrid model by taking additional corrections from higher order operators in supergravity. The potential is given by

$$V = \Lambda(1 + \alpha \ln x + \beta x^2), \quad (14)$$

where $x = \phi/M_{\text{pl}}$, and α is a positive dimensionless parameter. The value of the free parameter β can be either positive and negative. The potential is plotted in the top-left panel of Fig. 5 with different choices of parameters. With non-minimal derivative coupling the first and second slow-roll parameters are given by

$$\epsilon = M_{\text{pl}}^2 \frac{M^2 \left(\frac{\alpha}{x} + 2x\beta\right)^2}{2\Lambda(1 + x^2\beta + \alpha \ln[x])^2}, \quad (15)$$

$$\eta = M_{\text{pl}}^2 \frac{M^2 \left(-\frac{\alpha}{x^2} + 2\beta\right)}{\Lambda(1 + x^2\beta + \alpha \ln[x])^2}, \quad (16)$$

Compared with the minimal coupled case, one notes that variations of slow-roll parameters are strongly suppressed. Besides, when $\beta < 0$ the field potential develops a maximum hill. Inflation can occur by rolling down the field from

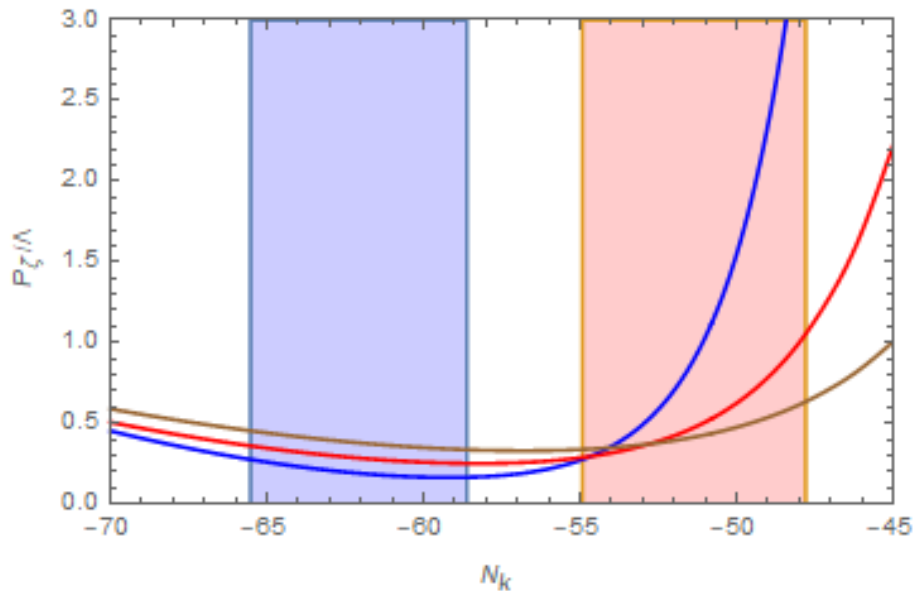


FIG. 3: Power spectrum of curvature perturbations for VHI with three parameter sets: $\mu_{VHI} = 0.0301$ and $\log_{10} x_{end} = -5.87$ (blue), $\mu_{VHI} = 0.0365$ and $\log_{10} x_{end} = -3.95$ (red), $\mu_{VHI} = 0.0415$ and $\log_{10} x_{end} = -3.00$ (brown).

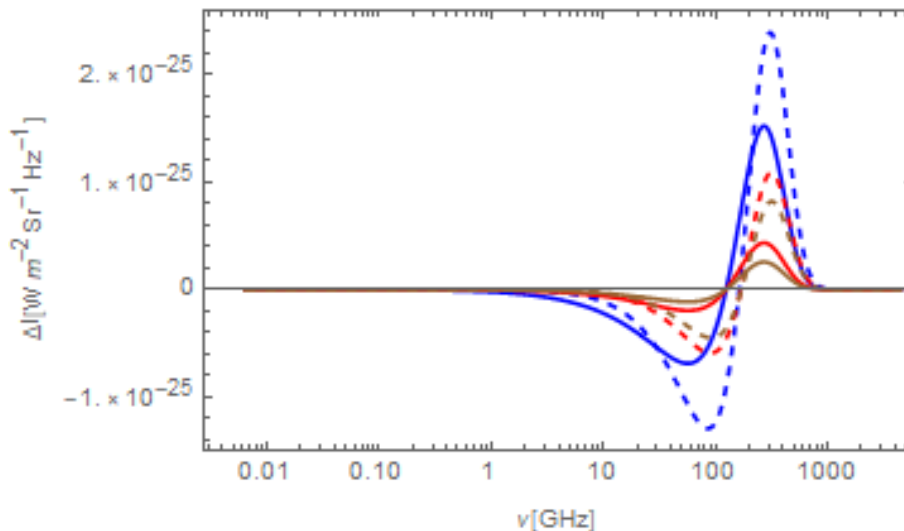


FIG. 4: The level of CMB distortion for VHI. The parameter sets are the same as in Fig. 3. Solid lines correspond to μ -distortions, whereas dash lines represent intermediate i -distortions.

both sides of the potential hill. However, the value of $\eta > 0$ is always negative, such that the $\beta < 0$ case is therefore not of interest, which is similar to the minimal coupled NCKI.

For $\beta > 0$, we look into the high-friction limit by setting $M = 0.01\sqrt{\Lambda}/M_{\text{pl}}$, and draw a contour diagram of scalar index at the distortion pivot scale $k = 42\text{Mpc}^{-1}$ in the plane of α and β , as shown in Fig. 6. The PLANCK-allowed region is between the two red lines. From this figure, we find that, to satisfy PLANCK constraints and generate a detectable distortion signal simultaneously, the parameter α must be much smaller than β . In this situation, the potential (14) has reduced to that of the VHI model. Therefore, this model may lead to 5σ detection of CMB distortion.

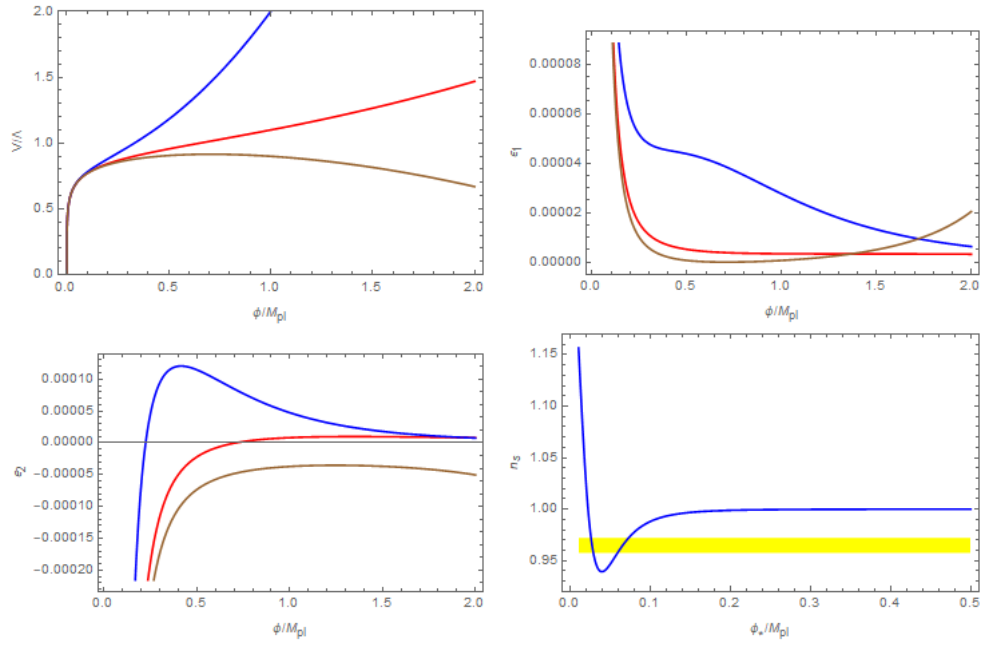


FIG. 5: Top left: Potential of the NCKI model. Top right and bottom left: first and second slow-roll parameter ϵ, η . The parameter sets for these three diagrams are: $\alpha = 0.1, \beta = 1$ (blue), $\alpha = 0.1, \beta = 0.1$ (red), and $\alpha = 0.1, \beta = -0.1$ (brown). Bottom right: spectral index value as a function of ϕ_* for $\alpha = 10^{-7}$ and $\beta = 600$.

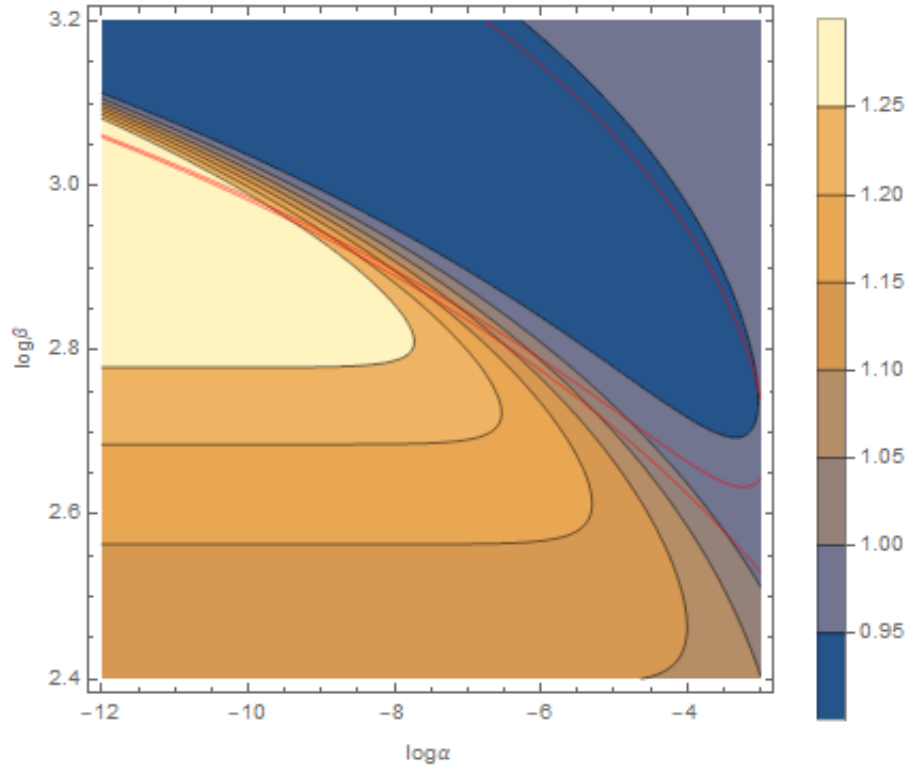


FIG. 6: Contours of spectral index values for NCKI. The area between the solid red lines is consistent with the spectral index at $k_p = 0.05 M_{\text{PC}}^{-1}$ at 95% C.L..

VI. GENERALIZED MSSM INFLATION (GMSSMI)

The Minimal Supersymmetric Standard Model (MSSM) is a minimal extension of the Standard Model with copious cosmological consequences. In Ref. [44], the authors argue that candidates for the inflaton can be provided by two combinations of flat directions, namely **LLe** and **udd**. The scalar potential for inflation can be parameterized as $V(\phi) = \Lambda \left[\left(\frac{\phi}{\phi_0}\right)^2 - \frac{2}{3}\left(\frac{\phi}{\phi_0}\right)^6 + \frac{1}{5}\left(\frac{\phi}{\phi_0}\right)^{10} \right]$. As for the minimally coupled case, the GMSSMI with the kinetic coupling also has an inflection point at $\phi = \phi_0$. Regions of red and blue spectrum are located on different sides of this point. However, in the classical slow-roll approximation, inflation approaches an infinite number of e-folds at the inflection point. The second criterion from Sec. III thus cannot be applied. Therefore, we consider the Generalized MSSM Inflation (GMSSMI) scenario, where the inflection point is approximately. Following Ref. [1], the potential of the GMSSMI model is parameterized as

$$V(\phi) = \Lambda \left(x^2 - \frac{2}{3}\alpha x^6 + \frac{1}{5}\alpha x^{10} \right), \quad (17)$$

where $x \equiv \phi/\phi_0$ and α is a dimensionless parameter that encodes the deviation from the MSSM inflation. If $\alpha > 1$, the potential develops a maximum. There are three possible inflationary field trajectories (towards both sides of the maximum, and from the large field regime towards decreasing field values). If $\alpha < 1$, the potential is monotonic. The field potential with different values of α is illustrated in Fig. 7. The slow-roll parameters read

$$\epsilon = M_{\text{pl}}^4 \frac{M^2}{\Lambda} \frac{6750(\alpha x^4(x^4 - 2) + 1)^2}{\phi_0^2 x^4 (\alpha x^4(3x^4 - 10) + 15)^3}, \quad (18)$$

$$\eta = M_{\text{pl}}^4 \frac{M^2}{\Lambda} \frac{450(\alpha x^4(9x^4 - 10) + 1)}{\phi_0^2 x^4 (\alpha x^4(3x^4 - 10) + 15)^2}, \quad (19)$$

where the slow roll approximation $3H^2 = V$ is applied. In the MSSM scenario, it suggests that $\Lambda \sim M_{\text{pl}}^{3/2} m_{\text{SUSY}}^{5/2}$ and $\phi_0 \sim M_{\text{pl}}^{3/4} m_{\text{SUSY}}^{1/4}$. For the minimally coupled case, inflation can only proceed in a fine-tuned region of $\alpha \simeq 1$, to satisfy the minimum of the first slow-roll parameter $\epsilon_{\text{min}} < 1$, and to create enough e-folds (c.f. Ref. [1]). With the non-minimal derivative coupling, the slow-roll parameters are suppressed, whereas the e-folds number is enhanced by a factor of $3H^2/M^2$. In the high friction limit where $M^2 \ll H^2$, the allowed region of α is much larger. We can still set the coupling constant $M = 0.01\sqrt{\Lambda}/M_{\text{pl}}$. The slow-roll parameters and the spectral index are then presented in Fig. 7. Inflation ends by violation of the slow-roll conditions when $\eta > 1$. The corresponding end point is $x_{\text{end}} = \sqrt[4]{0.0002M_{\text{pl}}^2/\phi_0^2}$. For applying the third criterion from Section III, we illustrate the spectral index in Fig. 8 in the plane (ϕ_0, α) for the two pivot scales $k_p = 0.05\text{Mpc}^{-1}$ and $k_d = 42\text{Mpc}^{-1}$. The potentially interesting region is all the area between the red lines in the figure. We select three representative parameter sets from this region, then evaluate the scalar power spectrum and the level of CMB distortions. The results are presented respectively in Figs. 9 and 10. In the third case, where $\phi_0 = 0.134M_{\text{pl}}$ and $\alpha = 0.825$, the amplitude at $k_d = 42\text{Mpc}^{-1}$ is about ten times more than that at Planck scales, and the corresponding $\mu = 5.3 \times 10^{-8}$. Thus, the signal of the distortions can be detected by a PIXIE-like experiment at 5σ confidence level. As for the HVI, the intermediate *i*-type signal is stronger than that of the μ -type one. We also note that the value of parameter ϕ_0 and expectation values of inflaton field are sub-Planckian. However, in Ref. [44], it suggests $\phi_0 \simeq 10^{-4}M_{\text{pl}}$.

In order to be in agreement with the MSSM scenario, one needs to turn on an extremely strong kinetic coupling. We can take $M = 10^{-5}\sqrt{\Lambda}/M_{\text{pl}}$ as an example. In this case, the end point of inflation is $x_{\text{end}} = 3.76 \times 10^{-3}\sqrt{M_{\text{pl}}/\phi_0}$. The corresponding plane diagram of the value of the spectral index is presented in Fig 11. The interesting parameter regime in the scope of this paper is from $\log_{10}(\phi_0/M_{\text{pl}}) \approx -3.90$ to $\log_{10}(\phi_0/M_{\text{pl}}) \approx 3.84$, and $\alpha > 0.244$. Then, we choose a point inside the region $n_s(k_d) > 1.25$, such as $\log_{10}(\phi_0/M_{\text{pl}}) = -3.87$ and $\alpha = 0.818$. The resulting CMB distortion is $\mu = 5.07 \times 10^{-8}$ which can be detected at 5σ . Moreover, the field value at horizon exit at 60 e-folds reads $\phi(N_k = 60) \approx 1.25\phi_0 = 1.69 \times 10^{-4}M_{\text{pl}}$. Hence the inflaton field runs at sub-Planckian scales during the inflation process. Compared with the $M = 0.01\sqrt{\Lambda}/M_{\text{pl}}$ case above and the minimally coupled case in Ref. [22], it is easy to find that the kinetic coupling can suppress the value of ϕ_0 and the inflaton field. The stronger the kinetic coupling is, the smaller ϕ_0 will be.

VII. GENERALIZED RENORMALIZABLE INFLECTION POINT INFLATION (GRIFI)

As for MSSM inflation, the renormalizable inflection point inflation features an exact inflection point to cause an eternal inflation. The number of e-folds diverges at this point. It immediately leads us to Generalized Renormalizable

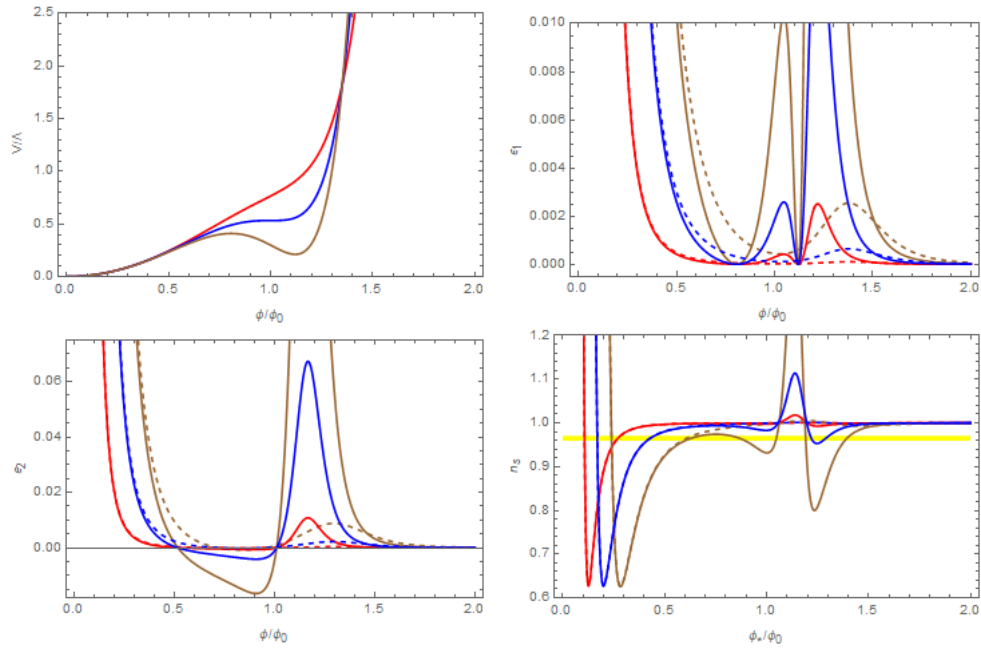


FIG. 7: Field potential (top left) for the generalized MSSM inflation model for $\alpha = 0.5$ (red), 1 (blue), and 1.5 (brown). First and second slow-roll parameters (respectively top right and bottom left) and spectral index value as a function of ϕ_* (bottom right), for the parameters $\phi_0 = 2.5 M_{\text{pl}}$ (red), $\phi_0 = 1 M_{\text{pl}}$ (blue); and $\phi_0 = 0.5 M_{\text{pl}}$ (brown), and $\alpha = 1.5$ (solid) or $\alpha = 0.5$ (dashed).

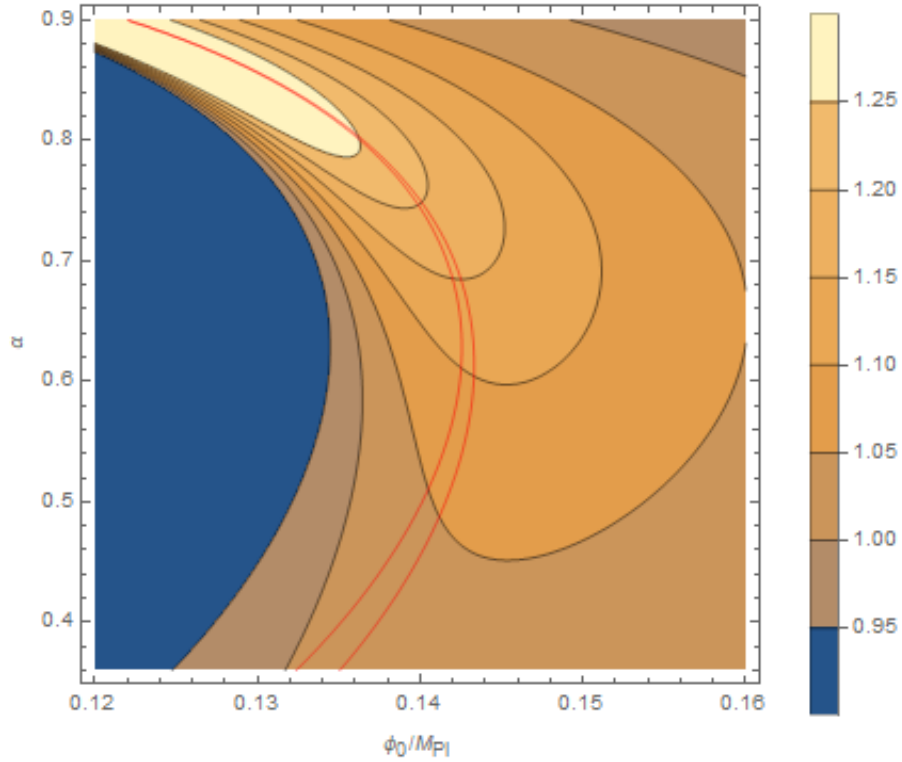


FIG. 8: Spectral index values for the GMSSMI at $k_d = 42 \text{Mpc}^{-1}$. The area between the solid red lines is consistent with the PLANCK constraints.

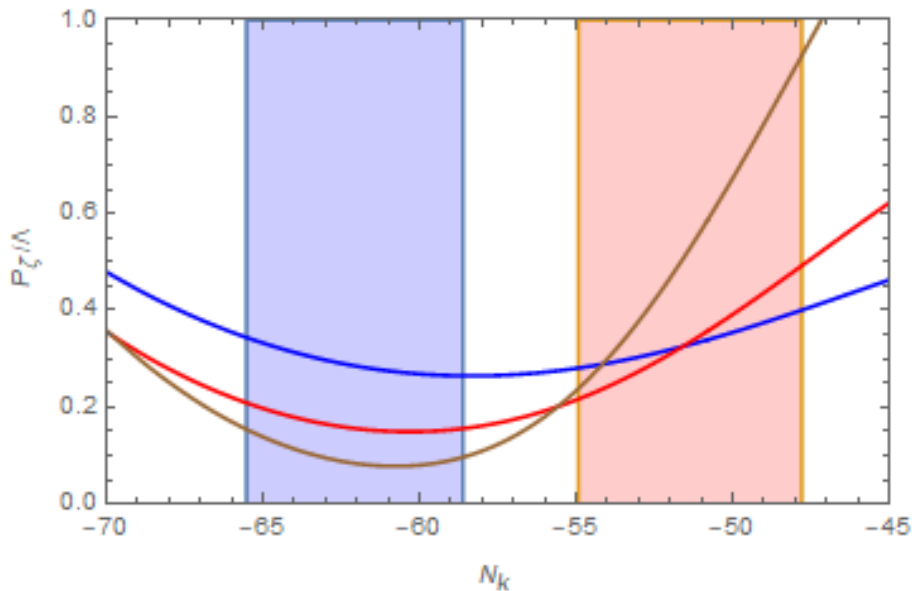


FIG. 9: Power spectrum of curvature perturbations for the GMSSMI for three parameter sets: $\phi_0 = 0.140M_{\text{pl}}$ and $\alpha = 0.470$ (blue), $\phi_0 = 0.143M_{\text{pl}}$ and $\alpha = 0.660$ (red), $\phi_0 = 0.134M_{\text{pl}}$ and $\alpha = 0.825$ (brown). The amplitude can be normalized by a suitable choice of Λ .

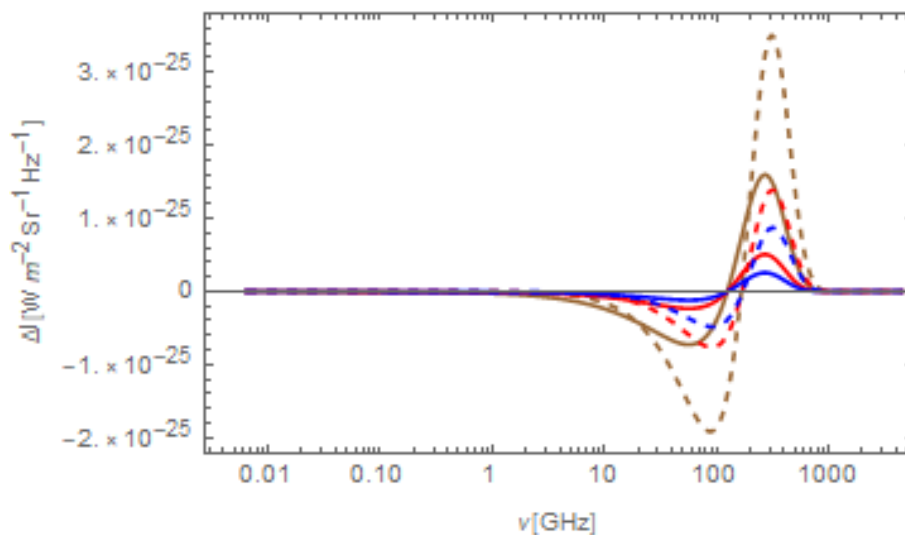


FIG. 10: Spectrum of intermediate and μ -distortions (respectively dashed and solid line) for the GMSSMI, same parameters as in Fig 9. They correspond to $\mu = 8.7 \times 10^{-9}$ (blue), $\mu = 1.7 \times 10^{-8}$ (red), $\mu = 5.3 \times 10^{-8}$ (brown). The signal is detectable for PIXIE at more than 5σ in the third case.

Inflection Point Inflation (GRIPi), where the inflection point is approximate. The GRIPi is similar to GMSSMI, and differs only at the powers of the inflaton. The field potential can be expressed as

$$V(\phi) = \Lambda \left(x^2 - \frac{4}{3}\alpha x^3 + \frac{1}{2}\alpha x^4 \right), \quad (20)$$

where $x = \phi/\phi_0$, and α is a dimensionless parameter. The field potential is presented in Fig. 12. When $\alpha < 1$, it is a monotonically increasing function of the field. As for GMSSMI, when $\alpha > 1$, the potential develops a maximum with

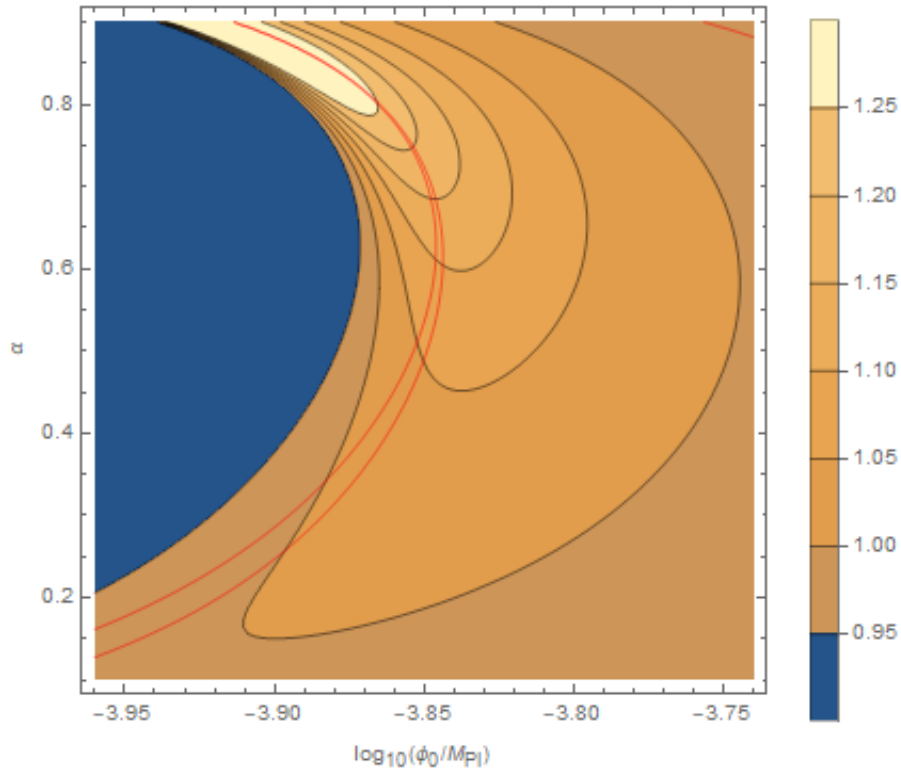


FIG. 11: Spectral index values for the GMSSMI with $M = 10^{-5}\sqrt{\Lambda}/M_{\text{pl}}$ at $k_d = 42\text{Mpc}^{-1}$. The area between the solid red lines is consistent with the PLANCK constraints.

three possible inflationary regimes. The slow-roll parameters are given by

$$\epsilon = M_{\text{pl}}^4 \frac{M^2}{\Lambda} \frac{(2x - 4x^2\alpha + 2x^3\alpha)^2}{2\phi_0^2 x(x^2 - \frac{4x^3\alpha}{3} + \frac{x^4\alpha}{2})^3}, \quad (21)$$

$$\eta = M_{\text{pl}}^4 \frac{M^2}{\Lambda} \frac{72(1 + x(-4 + 3x)\alpha)}{\phi_0^2 x^4(6 + x(-8 + 3x)\alpha)^2}. \quad (22)$$

Since the rescaled field x is dimensionless, we can fix the coupling constant as $M = 0.01\sqrt{\Lambda}/M_{\text{pl}}$, such that inflation ends by violation of slow-roll conditions at $x_{\text{end}} = \sqrt[4]{2 \times 10^{-4} M_{\text{pl}}^2/\phi_0^2}$. Then we can obtain the field value ϕ_k for each given mode at horizon exit by numerically integrating the Klein-Gordon equation in the slow-roll approximation. The spectral index predictions in the two-dimensional parameter space for the pivot scale $k_d = 42\text{Mpc}^{-1}$ are illustrated in Fig. 13. The band between the red lines is the available region consistent with PLANCK data. The potentially interesting region is the overlap between this band and the region where $n_s > 1$. We then evaluate the scalar amplitude and the level of distortions for three parameter sets. The results are shown in Figs. 14 and 15. When $\phi_0 = 0.125$, and $\alpha = 0.987$, CMB distortions are available at more than 5σ confidence for a PIXIE-like experiment. However, one may note that the value of ϕ_0 is still much greater than that required by MSSM, where $\phi_0 \simeq 10^{-5}M_{\text{pl}}$ [45]. In order to get such a small value of ϕ_0 , one needs to set the coupling constant to be $M = 10^{-6}\sqrt{\Lambda}/M_{\text{pl}}$. The corresponding plane plot for the value of spectral index n_s at $k_d = 42\text{Mpc}^{-1}$ is shown in Fig. 16.

VIII. RUNNING-MASS INFLATION (RMI)

Running-mass Inflation (RMI) also comes from a supersymmetric framework [1, 46–49]. A flat direction of the potential is lifted when the supersymmetry is explicitly broken by a soft term. It gives a logarithmic correction to the

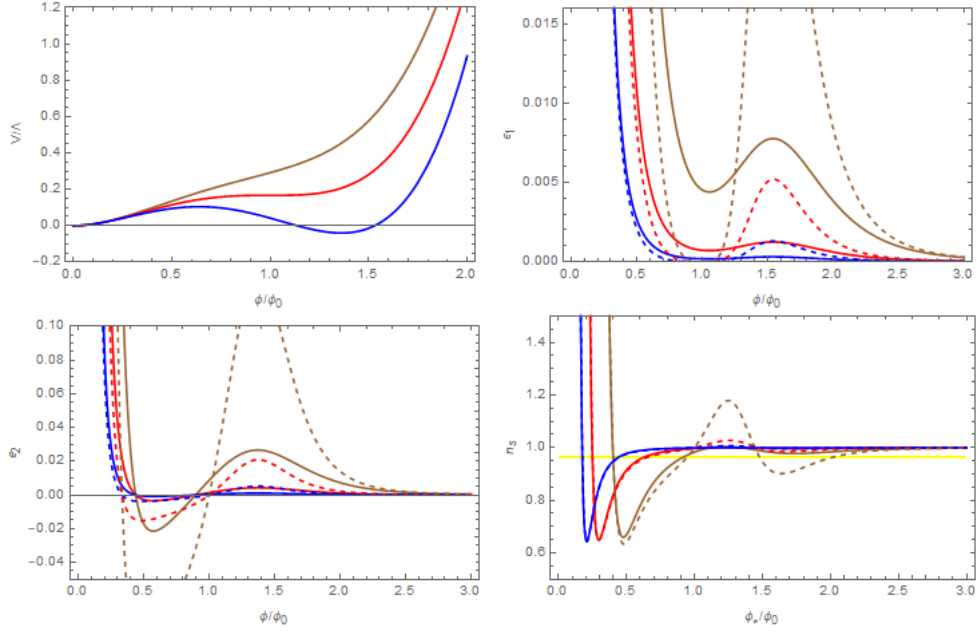


FIG. 12: Generalized Renormalizable Inflection Point Inflation (GRIPI) potential (top left) for $\alpha = 0.85$ (brown), $\alpha = 1$ (red), and $\alpha = 1.15$ (blue). First and second slow-roll parameters (respectively top right and bottom left) and spectral index value as a function of ϕ_* (bottom right), for $\phi_0 = (0.2, 0.5, 1)M_{\text{Pl}}$ (respectively brown, red and blue) and $\alpha = 0.85, 1$ (respectively solid and dashed).

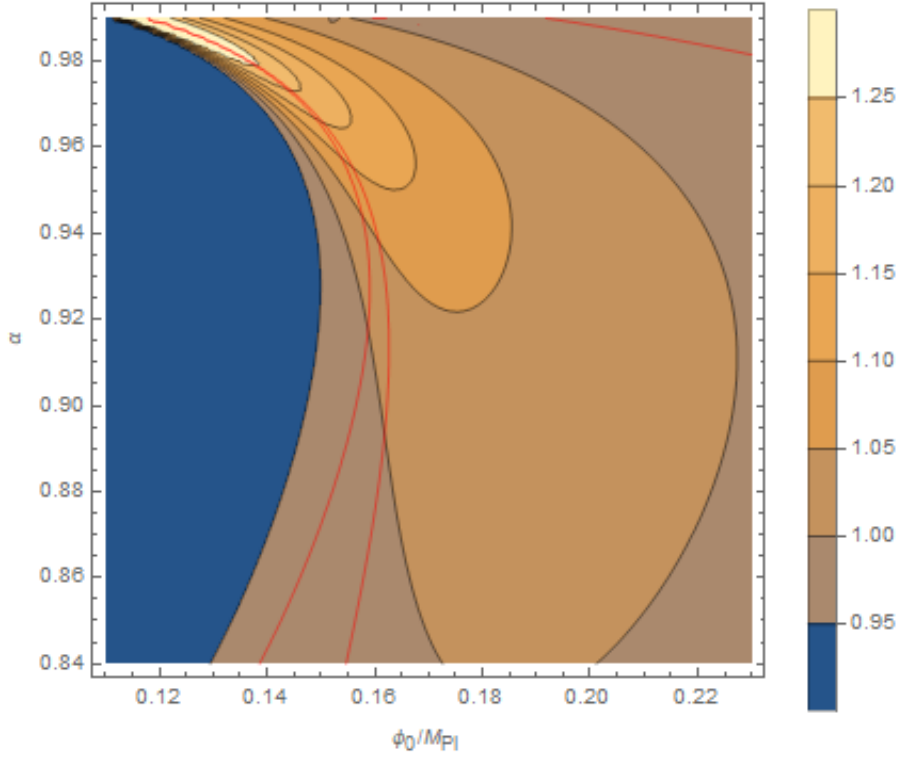


FIG. 13: Spectral index value in the parameter space (ϕ_0, α) for GRIPI, for the pivot scales of CMB distortions $k_d = 42\text{Mpc}^{-1}$. The area between the solid red lines is consistent with PLANCK constraints.

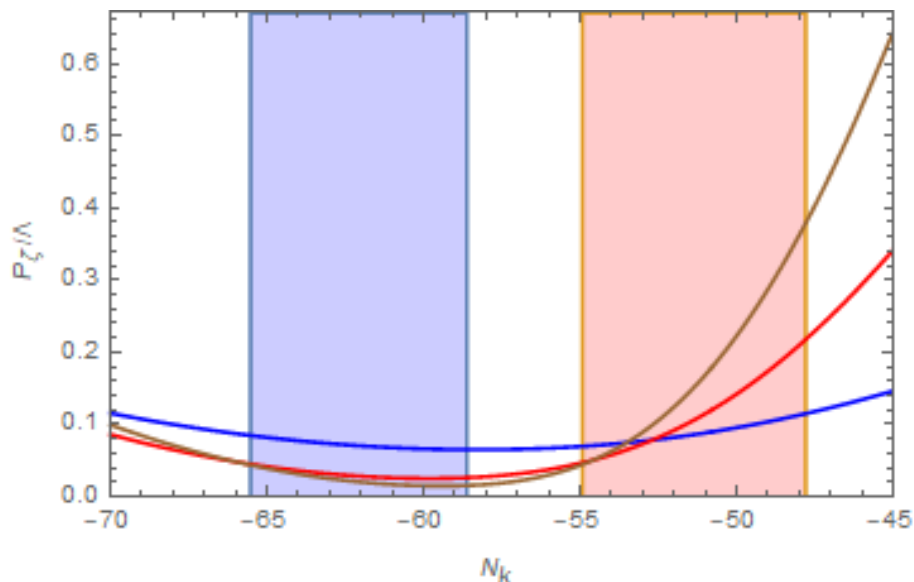


FIG. 14: Power spectrum of curvature perturbation for GRIPI, for $\phi_0 = 0.161$, and $\alpha = 0.94$ (blue), for $\phi_0 = 0.141$, and $\alpha = 0.977$ (red), for $\phi_0 = 0.125$, and $\alpha = 0.987$ (brown).

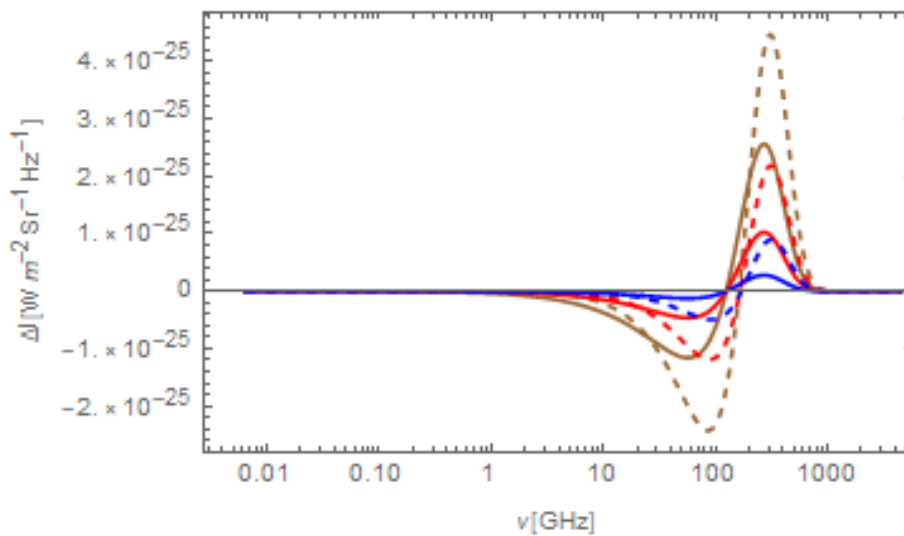


FIG. 15: Intermediate (dashed) and μ -type distortion for the GRIPI, same parameters as in Fig. 14. They correspond to $\mu = 9.34 \times 10^{-9}$ (blue), $\mu = 3.44 \times 10^{-8}$ (red), and $\mu = 8.60 \times 10^{-8}$ (brown).

tree-level inflaton mass. Then the potential reads

$$V(\phi) = \Lambda \left[1 - \frac{c}{2} \left(-\frac{1}{2} + \ln \frac{\phi}{\phi_0} \right) \frac{\phi^2}{M_{pl}^2} \right], \quad (23)$$

where ϕ_0 is the renormalization scale and c is a dimensionless parameter. The value of c can be either positive or negative. These different possibilities are illustrated in Fig. 17. If $c > 0$, the potential develops a maximum at $\phi = \phi_0$. There are two possible inflationary regimes: (i) from the maximum towards the decreasing field values (RMI1); (ii) from the maximum towards the increasing field values (RMI2). If $c < 0$, there is a minimum located at $\phi = \phi_0$ with two inflationary trajectories. Inflation can proceed from the small field values regime towards the minimal (RMI3) or

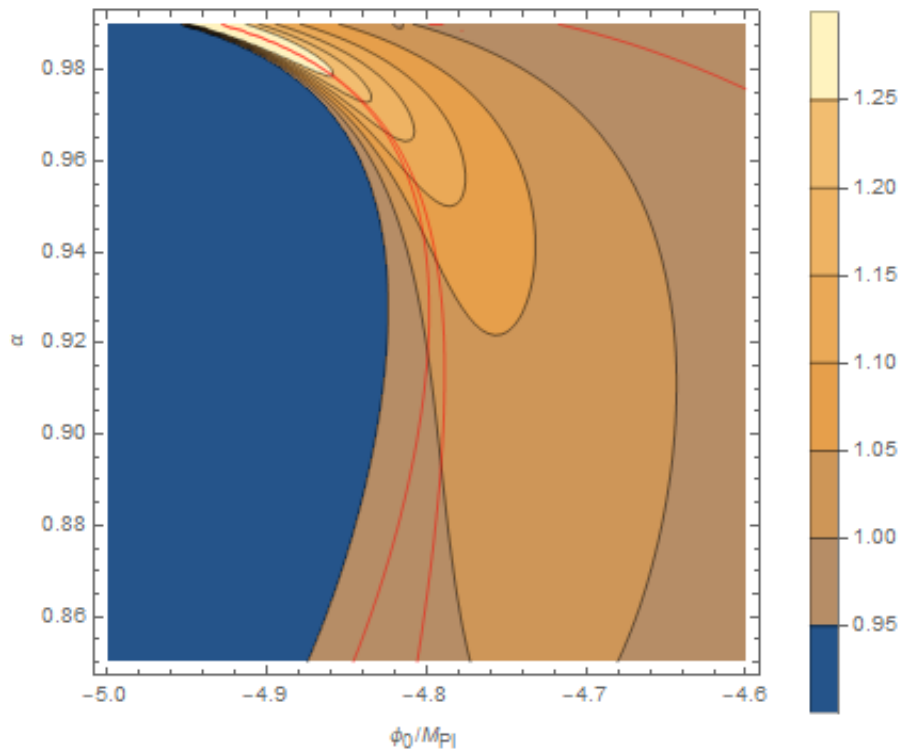


FIG. 16: Same as in Fig. 13 with the coupling constant $M = 10^{-6}\sqrt{\Lambda}/M_{\text{pl}}$.

from the minimum towards the increasing field values (RMI4). The slow-roll parameters are given by

$$\epsilon = M_{\text{pl}}^2 \frac{M^2 \left(-\frac{cx}{2} - cx\left(-\frac{1}{2} + \log\left[\frac{x}{\phi_0}\right]\right)\right)^2}{2\Lambda\left(1 - \frac{1}{2}cx^2\left(-\frac{1}{2} + \log\left[\frac{x}{\phi_0}\right]\right)\right)^3} \quad (24)$$

$$\eta = -M_{\text{pl}}^2 \frac{16cM^2\left(1 + \log\left[\frac{x}{\phi_0}\right]\right)}{\Lambda\left(4 + cx^2 - 2cx^2 \log\left[\frac{x}{\phi_0}\right]\right)^2} \quad (25)$$

where $x \equiv \phi/M_{\text{pl}}$. We set the derivative coupling $M = 0.01\sqrt{\Lambda}/M_{\text{pl}}$. The slow-roll parameters and spectral index value as a function of ϕ_* are demonstrated in Fig. 17. As for the original model [22], the RMI2 is irrelevant in the scope of the present paper, since the spectral index is always red. The other three regimes (RMI1, RMI3, and RMI4) allow one to satisfy observation constraints of n_s from the CMB anisotropies, and give rise to an enhanced spectrum amplitude at smaller scales. We then study these regimes in detail by integrating the slow-roll dynamics numerically.

A. RMI1: $c > 0$, $\phi < \phi_0$

As mentioned in Ref. [1], for the validity of the RMI model, inflation must end by a tachyonic waterfall instability. In the RMI1 regime, we parameterize the critical instability point as $\phi_c = c_2\phi_0$, where $c_2 < 1$ is a dimensionless parameter. In order to obtain the scalar power spectrum, we numerically integrate the Klein-Gordon equation in the slow-roll approximation. Spectral index values at the pivot scale of CMB distortions, $k_d = 42\text{Mpc}^{-1}$ in the parameter space (c_2, c) , are shown in Fig. 18 for the case of $\phi_0 = 0.1M_{\text{pl}}$. The area enclosed by red solid lines is in agreement with PLANCK observations. This area does not overlap with regions where $n_s > 1$ at the scale k_d . Therefore, the RMI1 regime cannot satisfy the PLANCK constraints and gives rise to a detectable spectral distortion simultaneously.

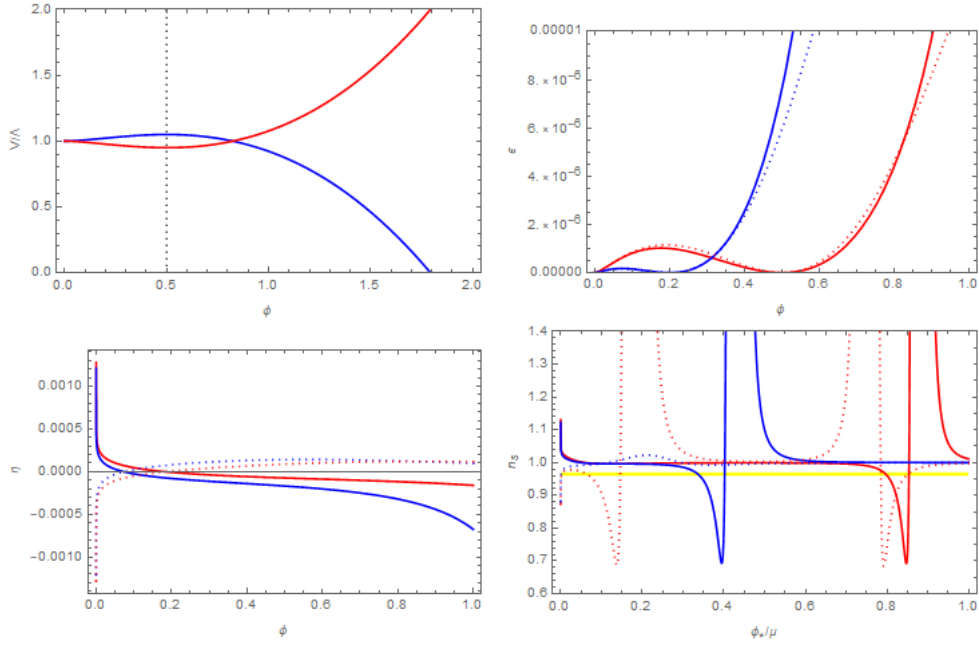


FIG. 17: Top left: field potential for the running-mass Inflation (RMI) for $\phi_0 = 0.5M_{\text{pl}}$, $c = 0.8$ (blue) and $c = -0.8$ (red). Top right and bottom left, respectively: first and second slow-roll parameter for the parameters $\phi_0 = 0.5M_{\text{pl}}$ (red), $\phi_0 = 0.2M_{\text{pl}}$ (blue), and $c = 0.8$ (solid) and $c = -0.8$ (dotted). Bottom left: spectral index value as a function of ϕ_* for the parameters $\phi_0 = 0.5M_{\text{pl}}$ (red), $\phi_0 = 0.2M_{\text{pl}}$ (blue); and $c = 40$ (solid), $c = -40$ (dotted).

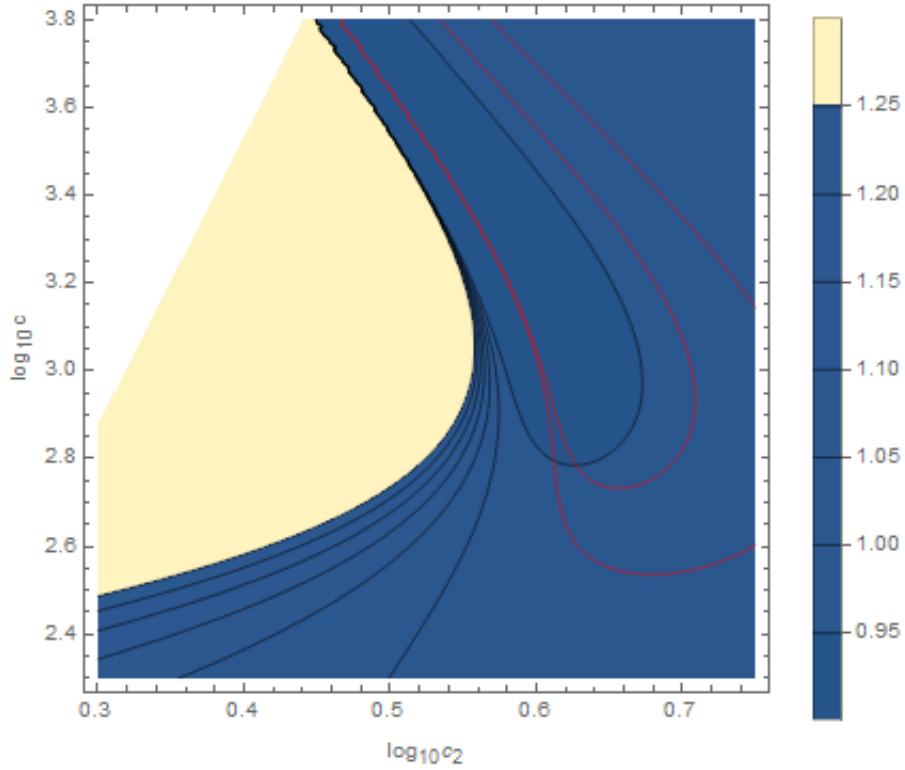


FIG. 18: Spectral index value for the RMI1 regime with $\phi_0 = 0.1M_{\text{pl}}$ at $k_d = 42\text{Mpc}^{-1}$. The area between the red lines is allowed by the PLANCK constraints at the pivot scale of CMB anisotropies $k_p = 0.05\text{Mpc}^{-1}$.

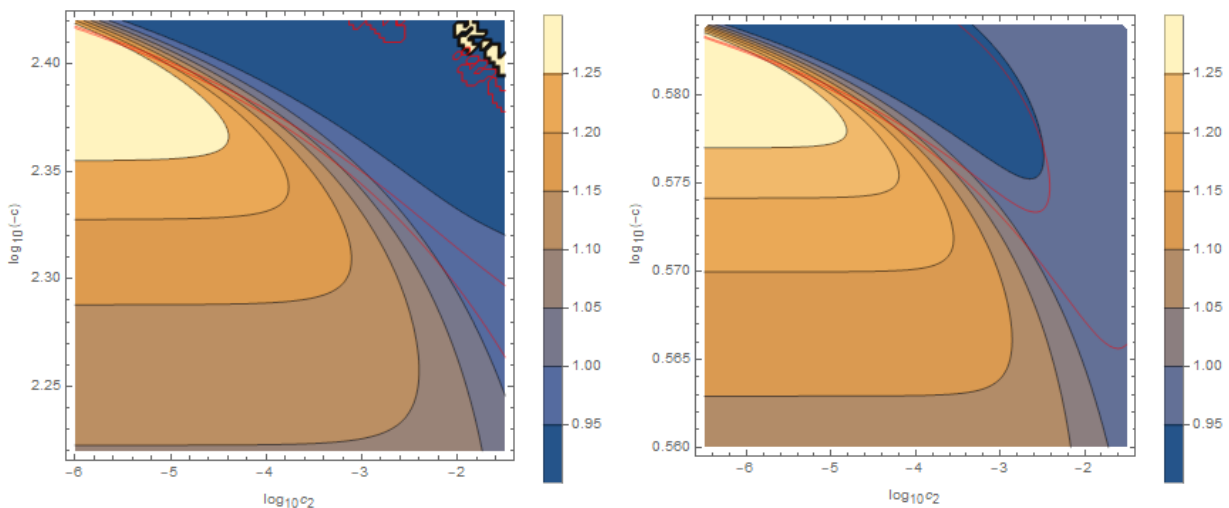


FIG. 19: Same as in Fig. 18, for the RMI3 regime with $\phi_0 = 0.1M_{\text{pl}}$ (left) and $\phi_0 = 1M_{\text{pl}}$ (right). The noises caused by numerical instability on the top right can be ignored.

B. RMI3 and RMI4: $c < 0$, $\phi < \phi_0$ or $\phi > \phi_0$

We combine the discussion of RMI3 and RMI4 together, because we can deal them in the same way and the results are similar. We define the critical tachyonic point as $\phi_c = (1 - c_2)\phi_0$. When $0 < c_2 < 1$, it corresponds to the RMI3 regime, whereas the RMI4 regime satisfies $c_2 < 0$. Contours of the spectral index at the scale k_d for the RMI3 and RMI4 regimes are presented in Figs. 19 and 20, respectively. Red solid lines represent the PLANCK 2σ confidence levels at the scale k_p . For both the RMI3 and RMI4 regimes, regions consistent with the PLANCK observations overlap with regions of blue tilted spectrum at the scale k_d , in cases of either $\phi_0 = 0.1M_{\text{pl}}$ or $\phi_0 = 1M_{\text{pl}}$. However, the case of $\phi_0 = 1M_{\text{pl}}$ is not preferred in the supersymmetric framework, since it may destroy the flatness of the potential by supergravity corrections. Comparing it with that of $\phi_0 = 0.1M_{\text{pl}}$ in Fig. 19 and 20, one can qualitatively conclude that the increasing of ϕ_0 would suppress the absolute value of c . In the case of $\phi_0 = 0.1M_{\text{pl}}$, the overlapped region correspond to $c \sim -10^{2.4}$, $c_2 < 0.01$ for the RMI3 regime, and to $c \sim -10^{2.4}$, $c_2 < -0.01$ for the RMI4 regime. We then evaluate the amplitude of scalar power spectrum and estimate the level of CMB distortions for two representative parameter sets from each regime. The results are plotted in Fig. 21 and Fig. 22. From these figures, we find that inflation taking place in either the RMI3 or RMI4 regime can lead to a detectable CMB distortion signal. However, field values at the end point are still fine-tuned, where $\phi_c \sim \phi_0$. The existence of kinetic coupling lifts up the absolute value of the parameter c .

IX. CONCLUSION

We have investigated the observational prospects of CMB spectral distortions generated by non-minimal derivative-coupled inflation in a model-oriented approach. In order to reveal the effects of kinetic coupling clearly, we consider the situations in the high friction limit $M^2 \ll H^2$. After examining all 49 models listed in Ref. [1], there are only 5 single-field models that can lead to increasing small-scale power, which is the necessary condition for a detectable distortion signal for a future PIXIE-like experiment. These models are hybrid inflation, non-canonical Kähler inflation, generalized MSSM inflation, generalized renormalization inflection point inflation, and running-mass inflation. For simultaneous consistency with PLANCK observations of the primordial scalar power spectrum and giving rise to a blue tilted spectrum at distortion scales, the potential regimes have been identified for all these models. We find that if the value of the spectral index at the pivot scale of distortions is large enough (usually the value is $n_s(k_d) \gtrsim 1.25$), all these models can lead to significant intermediate and μ -type distortions, which can be detected by a PIXIE-like experiment at 5σ confidence. The corresponding regions of parameter space are strongly tuned. Moreover, for each viable model, the signal of intermediate distortions is stronger than that of μ -type distortions, and inflation processes end at the sub-Planckian region. Compared with the minimally coupled models in Ref. [22], we also note that the kinetic coupling suppresses model parameters to be sub-Planckian for the VHI, GMSSMI, and GRIPI models. It helps the models to agree with theoretical considerations from the supersymmetric framework. For example, when

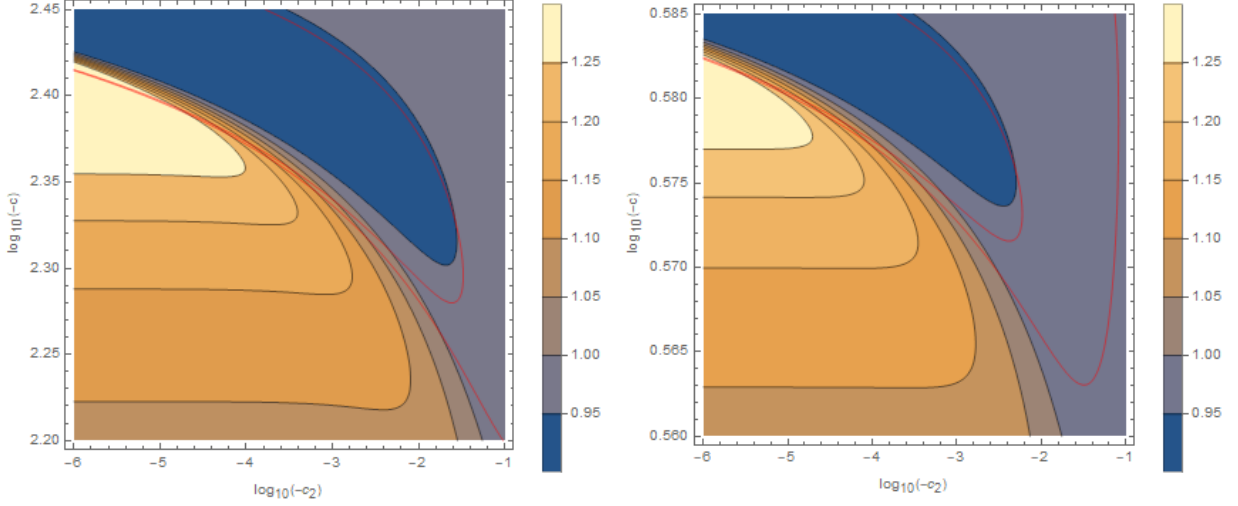


FIG. 20: Same as in Fig. 18, for the RMI4 regime with $\phi_0 = 0.1M_{\text{pl}}$ (left) and $\phi_0 = 1M_{\text{pl}}$ (right).

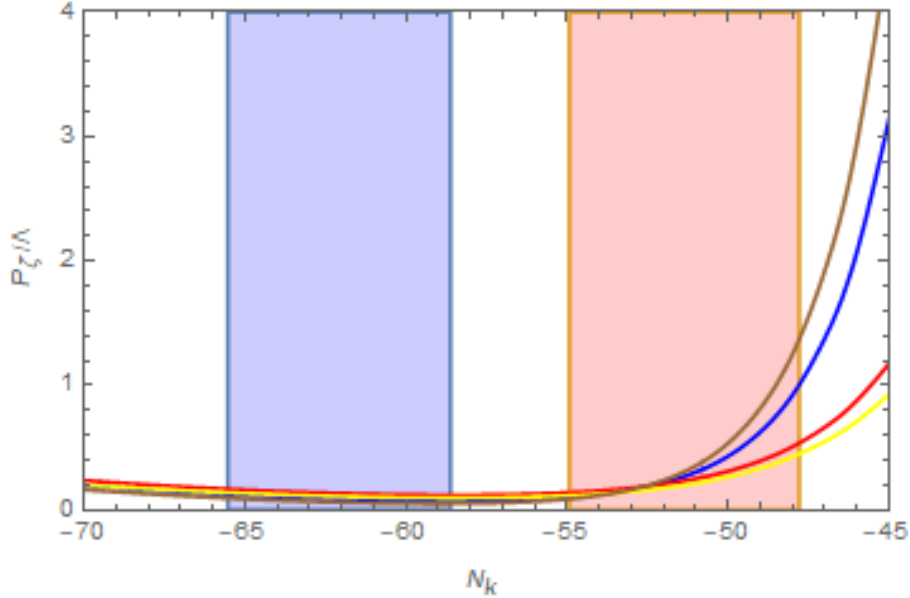


FIG. 21: Power spectrum of curvature perturbations for the RMI3 and RMI4 regimes with $c_2 = 10^{-5.983}$, $c = -10^{2.417}$ (RMI3, blue), $c_2 = 10^{-4.56}$, $c = -10^{2.39}$ (RMI3, red), $c_2 = -10^{-5.979}$, $c = -10^{2.415}$ (RMI4, brown), $c_2 = 10^{-3.89}$, $c = -10^{2.369}$ (RMI4, yellow).

$M = 10^{-6}\sqrt{\Lambda}/M_{\text{pl}}$, the value of parameter ϕ_0 for the GMSSMI model can drop off to the order of $10^{-5}M_{\text{pl}}$, which is required by the MSSM scenario [45]. For the NCKI model, it can lead to a detectable distortion signal only if $\beta \gg \alpha$, where the model becomes an approximate VHI model. For the RMI model, there are two inflationary regimes (RMI3 and RMI4) potentially detected by a PIXIE-like experiment. In the case of $\phi_0 = 0.1M_{\text{pl}}$, the model parameter c needs to be of the order of 10^2 in order to induce a blue spectrum at small scales. In the original model [50, 51], the absolute value of c should be of the order 10^{-1} to 10^{-2} . A larger value would not allow inflation to take place. However, with kinetic coupling, the slow-roll parameters are suppressed by a factor $M^2/3H^2$, such that the slow-roll conditions can be still preserved when $|c|$ is large.

If CMB distortions caused by damping of primordial perturbations are discovered by a PIXIE-like experiment, the kinetic coupled inflation scenarios are plausible candidates for the theoretical explanation. The corresponding observational constraints on model parameters will be very strong, since the regions of parameter space for increased small-scale power are fine-tuned. By contrast, if this signal cannot be detected, the experiment can only rule out very

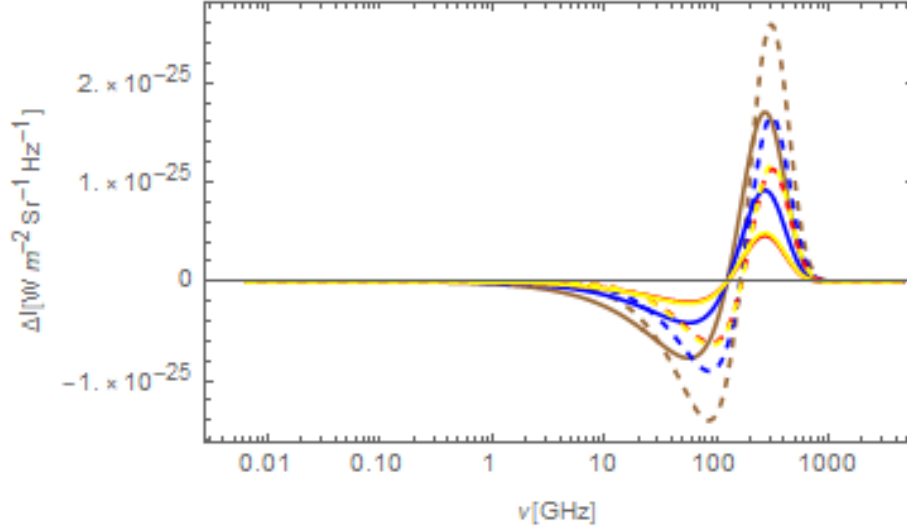


FIG. 22: Intermediate (dashed) and μ -type (solid) spectral distortion for the RMI model, same parameter values as in Fig. 21. They correspond to $\mu = 3.0 \times 10^{-8}$ (blue), $\mu = 1.5 \times 10^{-8}$ (red), $\mu = 5.7 \times 10^{-8}$ (brown), and $\mu = 1.6 \times 10^{-8}$ (yellow).

limited regions of parameter space for these models for the same reason. Nevertheless, a PIXIE-like experiment can provide an upper limit for scalar power amplitudes at small scales.

Acknowledgements

The authors warmly thank Björn Garbrecht, Sébastien Clesse, Yungui Gong, and Qing Gao for useful discussions and comments. RD and YZ received support from the National Natural Science Foundation of China (Grant No. 11705132) and the Fundamental Research Funds for the Central Universities (WUT:2018IVB018).

-
- [1] J. Martin, C. Ringeval, and V. Vennin (2013), 1303.3787.
 - [2] Y. Akrami et al. (Planck) (2018), 1807.06211.
 - [3] N. Aghanim et al. (Planck) (2018), 1807.06209.
 - [4] T. Bringmann, P. Scott, and Y. Akrami, Phys.Rev. **D85**, 125027 (2012), 1110.2484.
 - [5] A. S. Josan, A. M. Green, and K. A. Malik, Phys.Rev. **D79**, 103520 (2009), 0903.3184.
 - [6] S. Furlanetto, A. Lidz, A. Loeb, M. McQuinn, J. Pritchard, et al. (2009), 0902.3259.
 - [7] J. R. Pritchard and A. Loeb, Phys.Rev. **D82**, 023006 (2010), 1005.4057.
 - [8] J. R. Pritchard and A. Loeb, Rept.Prog.Phys. **75**, 086901 (2012), 1109.6012.
 - [9] J. Chluba et al. (2019), 1903.04218.
 - [10] J. Chluba et al. (2019), 1909.01593.
 - [11] J. Chluba (2018), 1806.02915.
 - [12] J. Chluba and R. Sunyaev (2011), 1109.6552.
 - [13] J. Chluba (2013), 1304.6121.
 - [14] R. A. Sunyaev and R. Khatri, Int.J.Mod.Phys. **D22**, 1330014 (2013), 1302.6553.
 - [15] J. Chluba, Mon. Not. Roy. Astron. Soc. **460**, 227 (2016), 1603.02496.
 - [16] D. Fixsen, E. Cheng, J. Gales, J. C. Mather, R. Shafer, et al., Astrophys.J. **473**, 576 (1996), astro-ph/9605054.
 - [17] W. Hu, D. Scott, and J. Silk, Astrophys. J. **430**, L5 (1994), astro-ph/9402045.
 - [18] A. Kogut, D. Fixsen, D. Chuss, J. Dotson, E. Dwek, et al., JCAP **1107**, 025 (2011), 1105.2044.
 - [19] A. Kogut, M. H. Abitbol, J. Chluba, J. Delabrouille, D. Fixsen, J. C. Hill, S. P. Patil, and A. Rotti (2019), 1907.13195.
 - [20] P. Andr, C. Baccigalupi, A. Banday, D. Barbosa, B. Barreiro, et al. (2013), 1310.1554.
 - [21] P. Andre et al. (PRISM Collaboration) (2013), 1306.2259.
 - [22] S. Clesse, B. Garbrecht, and Y. Zhu, JCAP **1410**, 046 (2014), 1402.2257.
 - [23] T. Kobayashi, Rept. Prog. Phys. **82**, 086901 (2019), 1901.07183.
 - [24] C. Charmousis, E. J. Copeland, A. Padilla, and P. M. Saffin, Phys. Rev. Lett. **108**, 051101 (2012), 1106.2000.
 - [25] F. Darabi and A. Parsiya, Class. Quant. Grav. **32**, 155005 (2015), 1312.1322.

- [26] S. Sushkov, Phys. Rev. **D85**, 123520 (2012), 1204.6372.
- [27] B. Gumjudpai and P. Rangdee, Gen. Rel. Grav. **47**, 140 (2015), 1511.00491.
- [28] M. A. Skugoreva, S. V. Sushkov, and A. V. Toporensky, Phys. Rev. **D88**, 083539 (2013), [Erratum: Phys. Rev.D88,no.10,109906(2013)], 1306.5090.
- [29] G. W. Horndeski, Int. J. Theor. Phys. **10**, 363 (1974).
- [30] S. Capozziello, G. Lambiase, and H. J. Schmidt, Annalen Phys. **9**, 39 (2000), gr-qc/9906051.
- [31] S. V. Sushkov, Phys. Rev. **D80**, 103505 (2009), 0910.0980.
- [32] C. Gao, JCAP **1006**, 023 (2010), 1002.4035.
- [33] C. Germani and A. Kehagias, Phys. Rev. Lett. **105**, 011302 (2010), 1003.2635.
- [34] N. Yang, Q. Fei, Q. Gao, and Y. Gong, Class. Quant. Grav. **33**, 205001 (2016), 1504.05839.
- [35] I. Dalianis and F. Farakos (2015), poSCORFU2014,098(2015), 1504.06875.
- [36] Y. S. Myung, T. Moon, and B.-H. Lee, JCAP **1510**, 007 (2015), 1505.04027.
- [37] T. Qiu, Phys. Rev. **D93**, 123515 (2016), 1512.02887.
- [38] R. Herrera, J. Saavedra, and C. Campuzano, Gen. Rel. Grav. **48**, 137 (2016), 1609.03957.
- [39] I. Dalianis, G. Koutsoumbas, K. Ntrekis, and E. Papantonopoulos, JCAP **1702**, 027 (2017), 1608.04543.
- [40] K. Feng and T. Qiu, Phys. Rev. **D90**, 123508 (2014), 1409.2949.
- [41] P. Ade et al. (Planck Collaboration) (2013), 1303.5076.
- [42] R. Khatri and R. A. Sunyaev, JCAP **1209**, 016 (2012), 1207.6654.
- [43] A. D. Linde, Phys. Rev. **D49**, 748 (1994), astro-ph/9307002.
- [44] R. Allahverdi, K. Enqvist, J. Garcia-Bellido, and A. Mazumdar, Phys.Rev.Lett. **97**, 191304 (2006), hep-ph/0605035.
- [45] S. Hotchkiss, A. Mazumdar, and S. Nadathur, JCAP **1106**, 002 (2011), 1101.6046.
- [46] E. D. Stewart, Phys.Lett. **B391**, 34 (1997), hep-ph/9606241.
- [47] E. D. Stewart, Phys.Rev. **D56**, 2019 (1997), hep-ph/9703232.
- [48] L. Covi, D. H. Lyth, and L. Roszkowski, Phys.Rev. **D60**, 023509 (1999), hep-ph/9809310.
- [49] L. Covi and D. H. Lyth, Phys.Rev. **D59**, 063515 (1999), hep-ph/9809562.
- [50] L. Covi, D. H. Lyth, and A. Melchiorri, Phys. Rev. **D67**, 043507 (2003), hep-ph/0210395.
- [51] L. Covi, D. H. Lyth, A. Melchiorri, and C. J. Odman, Phys.Rev. **D70**, 123521 (2004), astro-ph/0408129.